ACS APPLIED BIO MATERIALS

www.acsabm.org Article

Bioactive and Elastic Nanocomposites with Antimicrobial Properties for Bone Tissue Regeneration

Dina M. Ibrahim, Ehsan Shirzaei Sani, Alaa M. Soliman, Nooshin Zandi, Ebrahim Mostafavi, Ahmed M. Youssef, Nageh K. Allam, and Nasim Annabi*

Cite This: *ACS Appl. Bio Mater.* 2020, 3, 3313−3325 Read Online

ACCESS | Metrics & More | Article Recommendations | Supporting Information

ABSTRACT: Bone injuries represent a major challenge in the medical field. The commonly used treatments for bone regeneration rely on the use of bone grafts that are usually associated with complications such as donor site morbidity, disease transmission, high cost, and lack of availability. Bone tissue engineering has become a golden solution for the repair of bone injuries by regenerating the damaged biological tissues using biocompatible scaffolds. However, most of the tissue engineered scaffolds do not possess the combined properties of high elasticity, appropriate stiffness, biocompatibility, osteoinductivity, and antimicrobial properties. In this study, we engineered bioactive and antimicrobial nanocomposites that can promote bone formation while simultaneously provide a barrier against bacterial infections commonly associated with bone implants. We used PEGylated polyglycerol sebacate as nanocomposites base, which was functionalized with Laponite nanosilicates, a synthetic nanoclay, and an antimicrobial peptide (AMP). The successful synthesis of the PEGylated polyglycerol sebacate and Laponite incorporation within the nanocomposites were confirmed through nuclear magnetic resonance (NMR) and Fourier transform infrared spectroscopy (FTIR). The scaffolds had an elastic modulus and ultimate tensile strength within a range of 3.8−4.7 MPa and 1.5−3 MPa, respectively. Furthermore, the scaffolds loaded with antimicrobial peptide exhibited a significant antimicrobial activity against both Gram-negative (*Escherichia coli*) and Gram-positive (*Staphylococcus aureus*) bacteria. The in vitro cytocompatibility tests showed >90% viability of preosteoblast (W-20-17) cells. Moreover, in vitro differentiation assays demonstrated the scaffolds' ability to promote osteogenic differentiation of W-20-17. Collectively, the nanocomposites containing Laponite and antimicrobial peptide were proven to have osteoinductive and antimicrobial activity, making them desirable for bone tissue engineering applications.

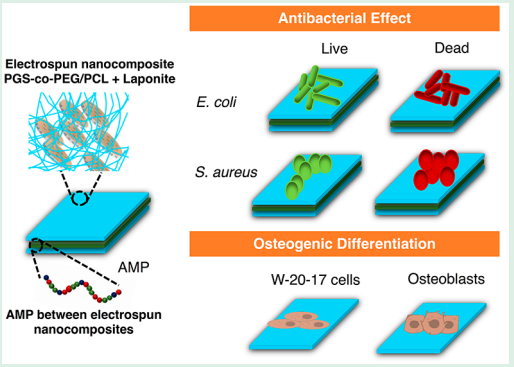

KEYWORDS: *bioactive nanocomposite, antimicrobial, Laponite, osteoinductive, elastic scaffolds*

1. INTRODUCTION

Following critical size bone injuries, the repair process generally relies on using bone grafts that can be autografts or allografts.[1,2] Autografts have several shortcomings, including donor site morbidity, infection, high cost, and chronic pain; whereas allografts convey the risk of disease transmission and host infection.[3] Bone tissue engineering has emerged as the golden standard in repairing bone defects to address the unmet need associated with current clinical treatment approaches.[1] The concept of bone tissue engineering relies on developing a scaffold that resembles the extracellular matrix (ECM) of native bone tissue. Ideally, this scaffold should provide mechanical support, facilitate the process of the bone formation, and be biodegradable and biocompatible.[1] Moreover, designing a scaffold with antimicrobial properties has become a critical requirement to overcome common microbial infections that can superimpose bone implants.[4,5]

Fibrous scaffolds have become particularly common for bone tissue engineering applications because of their biomimetic structure that can simulate the multiscale and hierarchical architecture of the ECM. This provides a favorable environment for rapid cell proliferation and differentiation within the scaffold.[6] One technique for fabricating fibrous scaffolds is electrospinning, which has emerged as a prevalent approach to produce fibrous scaffolds due to its versatility, low cost, and ability to produce scaffolds with tuned physical and mechanical properties.[7,8] Over the past years, various biomaterials have been explored for bone tissue engineering including metals, ceramics, and different types of natural and synthetic polymers.[1] Among these different biomaterials, synthetic polymers appear to be more beneficial due to their

Received: March 4, 2020
Accepted: April 21, 2020
Published: April 21, 2020

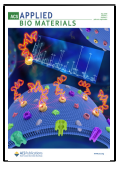

controllable physical properties (e.g., mechanical properties) and biocompatibility.[1] Nevertheless, introducing bioactive ingredients to these polymers has been explored to promote cell functions and enhance bone formation. For example, various bioactive molecules, such as zinc oxide (ZnO) nanoparticles and nanosilica ($nSiO_2$) have been combined with synthetic polymers to provide them with osteoinductive properties.[4,9]

In a clinical setting, bone implants are often at risk of bacterial colonization, which can lead to biofilm formation and eventually implant failure if not treated.[10] As a result, another important specification of bone regenerative scaffold is to be antimicrobial to prevent bacterial infections. Several strategies have been adopted by adding antimicrobial domains, such as metals (e.g., Ag), metal oxides (e.g., ZnO), and magnetic nanoparticles (e.g., Fe_3O_4) in addition to encapsulating antimicrobial drugs and antibiotics within scaffolds.[4,10−12] Despite the success of these antimicrobial agents, there are still concerns related to the toxicity for metals and antimicrobial resistance for known antibacterial drugs.[13,14] Therefore, it is necessary to combine all the desirable features for a successful bone tissue engineering scaffold, such as mechanical stability, osteoinductive, and antimicrobial properties.

Here, we engineer a biocompatible elastic scaffold with osteoinductive, and antimicrobial properties fabricated via the electrospinning technique. This serves as a versatile scaffold synthesis technique as bioactive nanoparticles and antimicrobial drugs can be easily incorporated during the electrospinning process. For this study, we used polycaprolactone (PCL) as a carrier polymer and a block copolymer of poly(glycerol sebecate) (PGS) and poly(ethylene glycol) (PEG) (PGS-*co*-PEG) to synthesize a robust nanocomposite scaffold. This block copolymer possessed tunable mechanical (e.g., elasticity) and degradation properties based on the PEG concentration.[15] To the extent of our knowledge, this is the first study, where PGS-*co*-PEG block copolymer is being investigated as a platform for hard tissue engineering. Recent studies have confirmed the positive effect of adequate elastic properties of the biomaterial in cell attachment, proliferation, and differentiation.[16,17] Laponite nanosilicates and an antimicrobial peptide (AMP) were incorporated in our elastic scaffold to provide a dual function of osteoinductive and antimicrobial properties, respectively. Laponite is an inorganic two-dimensional (2D) nanoplate. It has a chemical structure of $Na_{0.7}^{+}[(Mg_{5.5}Li_{0.3})Si_8O_{20}(OH)_4]_{0.7}^{-}$ with cytocompatible degradation products, such as magnesium ions (Mg^{2+}), orthosilicate ($Si(OH)_4$), and lithium (Li^{+}), that can enhance the osteogenic differentiation.[18]

In this work, we optimized three parameters: PEG to PGS ratio, copolymer to PCL ratio, and Laponite concentration, to engineer nanocomposites with tunable physical properties. Next, the physical properties (morphology, mechanical characteristics, and degradability) of the engineered nanocomposites were characterized. The antimicrobial activity of the nanocomposites was examined against *Escherichia coli* (*E. coli*) and *Staphylococcus aureus* (*S. aureus*) as models for Gram-negative and Gram-positive bacteria, respectively. Finally, the optimized nanocomposites were used to assess in vitro osteogenic differentiation of preosteoblast murine bone marrow stromal cells (W-20-17). The engineered nanocomposites are based on synthetic polymers with tunable mechanical/hydration properties. Moreover, the osteoinductive and antimicrobial functionalities of the engineered scaffolds make them ideal platforms for treatment of infected bone defects.

2. MATERIALS AND METHODS

2.1. Materials. PCL (M_w = 80 000) was purchased from Sigma-Aldrich. Sebacic acid (purity ≥ 98%) and glycerol (purity ≥ 99%) were obtained from Alfa Aesar, Germany. PEG (M_w = 1000) was purchased from Sigma-Aldrich, USA. 1,1,1,3,3,3-Hexafluoro-2-propanol (HFIP) (99.5%) was purchased from Oakwood Products, Inc., USA. Synthetic nanosilicates (Laponite XLG) were obtained from BYK Additives, Inc. (Rochester Hills, MI, USA), with dimensions of 20−50 nm diameter and 1 nm thickness. AMPs (Tet213, KRWWKWWRRC) were obtained from CSC Scientific, Inc. (Sunnyvale, CA, USA). Minimum essential medium α (MEM α) was obtained from Gibco, Thermo Fisher Scientific. Prestoblue kit for cells viability, live/dead viability kit, 4′,6-diamidino-2-phenylindole (DAPI), and Alexa Fluor 488−phalloidin were obtained from Invitrogen, Thermo Fisher Scientific. QuantiChrom calcium assay and alkaline phosphatase activity kits were purchased from BioAssays (Hayward, USA). cDNA synthesis kit was obtained from Roche. TAQMAN Master mix for qPCR was obtained from Applied Biosystems, Thermo Fisher Scientific. *Staphylococcus aureus* (*S. aureus*) and *Escherichia coli* (*E. coli*) were obtained from ATCC with strain numbers 12600 and 25922, respectively.

2.1.1. PGS-co-PEG and PGS Synthesis. PGS-*co*-PEG prepolymers were synthesized through a two-step polycondensation reaction as previously reported.[15] Briefly, sebacic acid and PEG were reacted for 24 h at 130 °C under the flow of Argon gas (Ar) and 50 mTorr vacuum. Next, glycerol was added, and the reaction was continued under reduced pressure for another 48 h to obtain the block copolymer. Three different copolymers were synthesized with PGS:PEG ratios of 1:10, 1:20, and 1:40 (PGS-*co*-10PEG, PGS-*co*-20PEG, and PGS-*co*-40PEG, respectively). PGS was synthesized as reported elsewhere[19] and was used as a control for chemical and physical characterizations.

2.2. Fabrication of Electrospun Scaffolds Containing Laponite and AMP. To fabricate the electrospun scaffolds, PGS, PGS-*co*-10PEG, PGS-*co*-20PEG, and PGS-*co*-40PEG prepolymers and PCL were dissolved in hexafluoro-2-propanol (HFIP) solvent. The total polymer concentration was kept at 18% (w/w) and the ratio of PGS, PGS-*co*-10PEG, PGS-*co*-20PEG, and PGS-*co*-40PEG to PCL was kept 2:1 to evaluate the effect of the PGS-*co*-PEG copolymers in the final fabricated scaffold. In this study, PCL was used as a carrier polymer to provide adequate chain entanglements during the electrospinning process of PGS and the copolymers. Four types of scaffold were fabricated, including PGS/PCL, PGS-*co*-10PEG/PCL, PGS-*co*-20PEG/PCL, and PGS-*co*-40PEG/PCL (referred to as PGS/PCL, 10/PCL, 20/PCL, and 40/PCL, respectively, in the paper). To synthesize Laponite-containing nanocomposites, PGS-*co*-40PEG and PCL were dissolved in HFIP at the previously mentioned concentration, and three different concentrations of Laponite (1%, 5%, and 10% (w/w)) were added to the solution to fabricate 40PEG/PCL/1%LA, 40PEG/PCL/5%LA, and 40PEG/PCL/10%LA nanocomposites (referred to as 40/PCL/1LA, 40/PCL/5LA, and 40/PCL/10LA, respectively, in the paper). The solutions were kept under constant stirring overnight followed by Laponite dispersion using a probe sonicator for 15 min in an ice bath. Finally, the polymer/Laponite solutions were electrospun using the following parameters: voltage of 20 kV, flow of 1 mL/h, and distance between the nozzle and collector was maintained at 15 cm. To fabricate the antimicrobial scaffolds, AMP was dissolved in Dulbecco's phosphate-buffered saline (DPBS) to obtain two concentrations: 0.2% and 0.4% (w/v). Using these AMP concentrations and 40PEG/PCL/5%LA prepolymer solution, two scaffolds were fabricated: 40PEG/PCL/5%LA/0.2% AMP and 40PEG/PCL/5%LA/0.4%AMP (referred to as 0.2AMP and 0.4AMP, respectively in the paper). Electrospun nanocomposites containing the two concentrations of AMP were fabricated through adding 30 μL of 0.2% (in case of 0.2AMP nanocomposite) and 0.4% (in case of 0.4AMP nanocomposites) of the AMP in DPBS solution in

https://dx.doi.org/10.1021/acsabm.0c00250
ACS Appl. Bio Mater. 2020, 3, 3313−3325

between the electrospun layers of the 40/PCL/5LA. The same previously mentioned electrospinning parameters were used. For easier handling, samples were collected on glass slides placed on top of a conductive plate collector. For further characterization, electrospun sheets were dried in a vacuum chamber overnight.

2.3. Chemical Characterization. *2.3.1. Gel Permeation Chromatography (GPC).* GPC (Agilent 1100 Series SEC system, Agilent Technologies) was preformed to determine the molecular weight of the PGS, PGS-*co*-10PEG, PGS-*co*-20PEG, and PGS-*co*-40PEG samples. Initially, 200 mg of each sample was dissolved in 2 mL of tetrahydrofuran (THF). Next, the solutions were filtered by using 0.45 μm filters. Samples were then loaded into the GPC device with a flow rate of 1 mL/min.

2.3.2. Nuclear Magnetic Resonance (^{1}H NMR). ^{1}H NMR analysis (JEOL GSX-500 NMR spectrometer) was executed to verify the presence of the PEG within the synthesized PGS-*co*-PEG polymers. After PGS, PGS-*co*-10PEG, PGS-*co*-20PEG, and PGS-*co*-40PEG prepolymers were dissolved in deuterated chloroform ($CDCl_3$), the ^{1}HNMR spectra were obtained at 500 MHz. The data were processed and evaluated using Delta NMR software (JEOL USA, Inc.). The assignment of the peaks in both PGS and PGS-*co*-PEG spectra is reported elsewhere.[15]

2.3.3. Fourier Transform Infrared (FTIR). FTIR was performed with attenuated total reflection and the spectra were recorded in transmittance mode over a wavenumber range of 500−4000 cm^{-1} (Vertex70 FTIR Spectrometer). The newly synthesized polymers with different compositions (e.g., PGS/PCL, 10/PCL, 20/PCL, 40/PCL, 40/PCL/1LA, 40/PCL/5LA, and 40/PCL/10LA) were mixed with KBr to form a pellet to be used in FTIR analysis.

2.4. Physical Characterization. *2.4.1. Morphology.* Morphology of the scaffolds was assessed using scanning electron microscopy (SEM) (ZEISS Leo Supra55 field emission SEM). Scaffolds were first coated with gold using a sputter coater at 20 mA for 2 min (LADD Hummer 8 Sputter Coater). Images of the scaffolds were captured at an accelerating voltage of 8 kV. Fiber diameters and pore sizes were measured using ImageJ software. For each group, 100 fibers from three different samples were assessed to obtain the average fiber diameters.

2.4.2. Mechanical Properties. The mechanical properties of the scaffolds were measured using a uniaxial mechanical tester (Instron 5542) as described previously.[20] Briefly, samples were first cut into rectangular strips (12 mm × 4.5 mm) and then incubated in DPBS for 2 h. Thickness was determined using a digital caliper (70−100 μm). For tensile testing, both ends of each sample were placed between double sided tape (ARcare 90445, clear polyester double-sided adhesive tape) and placed between the tensile grips of the mechanical tester. A strain rate of 1 mm/min was applied to each sample until failure. The linear (first 5−15%) portion of the stress−strain curves ($n \geq 3$) was used to calculate the elastic moduli.

2.4.3. Degradation. In vitro degradation of the scaffolds was evaluated by placing square samples ($n \geq 3$) (1 cm × 1 cm) in 1 mL of DPBS at 37 °C for 28 days. The specimens' weight was measured before the experiment. Following incubation for 1, 3, 5, 7, 14, or 28 days, the weight of the samples was measured after freeze-drying overnight. The weight loss was measured using the following equation[21]

$$\text{weight loss } (\%) = \frac{W_i - W_t}{W_i} \times 100$$

where W_i is the initial weight and W_t is the weight after the designated time points.

2.5. Biological Assessment. *2.5.1. In Vitro Cell Culture.* Pre-osteoblast murine bone marrow stromal cells (W-20-17) were cultured in a humidified atmosphere at 37 °C and 5% CO_2 in MEM α. The media was supplemented with penicillin/streptomycin (1% v/v) and fetal bovine serum (FBS) (10% v/v). The cells were used at 70% confluency for scaffold seeding. Scaffolds were cut into square samples (0.5 cm × 0.5 cm) and mounted on glass slides for easier handling. Prior to in vitro assessment, scaffolds were sterilized through soaking in 70% ethanol for 30 min, followed by UV exposure for another 30 min on both sides. Finally, each scaffold was seeded with 9.5×10^4 cells. The cell-seeded scaffolds were maintained in a humidified atmosphere at 37 °C and 5% CO_2 for future cell viability, proliferation and adhesion studies.

2.5.2. Cell Viability and Proliferation. The viability of cells seeded on scaffolds after 1, 3, and 5 days was evaluated using a live/dead cell viability kit according to the manufacturer's instructions.[22] Briefly, cell-seeded scaffolds were stained with ethidium homodimer-1 (EthD-1, 2 μL/mL in DPBS) for dead cells (red) and calcein AM (0.5 μL/mL in DPBS) for live cells (green). Next, after 15 min incubation at 37 °C, the stain was removed through washing with DPBS three times. Finally, the samples were imaged using an inverted fluorescence microscope (Zeiss Axio Observer Z1). Using ImageJ software, cell viability percentage was estimated by dividing the number of live cells by the total number of cells.

Metabolic activity of the cells was determined using a PrestoBlue kit following the manufacturer's protocol. Briefly, PrestoBlue solution was added to the media at days 1, 3, or 5 post-seeding to constitute 10% of the whole media in the wells. Subsequently, cells were incubated for 45 min at 37 °C. A microplate reader (Bio-Tek Inc.) was used to measure fluorescence intensity of the solutions at 590−615 nm emission and 535−560 nm excitation ($n \geq 3$).

2.5.3. Cell Adhesion and Spreading. To evaluate the adhesion and spreading of W-20-17 cells on the surface of the scaffolds, 4′,6-diamidino-2-phenylindole (DAPI) and Alexa Fluor 488−phalloidin staining were used.[23] Cells seeded on scaffolds were fixed in 4% (v/v) paraformaldehyde for 20 min at days 1, 3, and 5 post-seeding. Next, to increase the cells permeability and to block non-specific binding, cells were treated with 0.1% (w/v) Triton X-100 solution in DPBS for 45 min and 1% (w/v) bovine serum albumin (BSA) solution in DPBS for 2 h, respectively. Subsequently, cells were incubated with Alexa Fluor 488-phalloidin in 0.1% (w/v) BSA at 37 °C (1:200 dilution) for 45 min to stain the actin cytoskeleton. Next, cells were counter-stained with DAPI (1 μL/ml in DPBS) by incubating for 5 min at 37 °C to stain the nuclei of cells. Finally, the samples were washed with DPBS three times and visualized with an inverted fluorescence microscope (Zeiss Axio Observer Z1) ($n \geq 3$). DAPI stained nuclei were quantified using ImageJ software.

2.5.4. Alizarin Red Staining (ARS). The samples (40/PCL and 40/PCL/5LA) were washed with DPBS, followed by a 20 min fixation in 4% paraformaldehyde after 7 days of culture. Next, they were washed with deionized (DI) water before staining with a 2% (w/v) solution of Alizarin Red (pH 4.1−4.3) for 10 min at 37 °C. Alizarin Red solution was then removed, and samples were washed with DI water and imaged using an inverted microscope (Nikon Eclipse, Ti-E, Nikon Corporation) ($n \geq 3$).

2.5.5. Calcium Deposition Assay. Calcium biomineralization was quantified using a QuantiChrom Calcium Assay Kit according to the manufacturer's instructions. The assay is based on the formation of a stable blue complex between free calcium and phenolsulfonphthalein dye that can be measured by using a microplate reader at 612 nm.[24] Briefly, cell-seeded scaffolds (40/PCL and 40/PCL/5LA) were washed with DI H_2O to remove calcium ions from the media. Subsequently, scaffolds were homogenized in 0.6 M HCl for 4 h on a shaker at room temperature. Next, cell lysates were centrifuged at 12 000 rpm for 3 min, and 5 μL of the supernatant of each sample was mixed with 200 μL of working solution. After 3 min incubation at room temperature, absorbance was measured at 612 nm using a microplate reader (Bio-Tek Inc.). Calcium concentrations were determined from a previously developed standard calibration curve derived from known calcium concentrations ranging from 0 to 20 mg/dL ($n \geq 3$).

2.5.6. Alkaline Phosphatase Activity Assay. Evaluation of alkaline phosphatase (ALP) activity, an early marker of osteoblastic differentiation, was performed on cell-seeded scaffolds at 1, 4, or 7 days of culture using a QuantiChrom alkaline phosphatase activity assay. This assay is based on the hydrolysis of *p*-nitrophenyl phosphate (pNPP) substrate. Cell-seeded scaffolds (40/PCL and 40/PCL/5LA) were first washed with DPBS and then incubation with 0.2% Triton for 20

https://dx.doi.org/10.1021/acsabm.0c00250
ACS Appl. Bio Mater. 2020, 3, 3313−3325

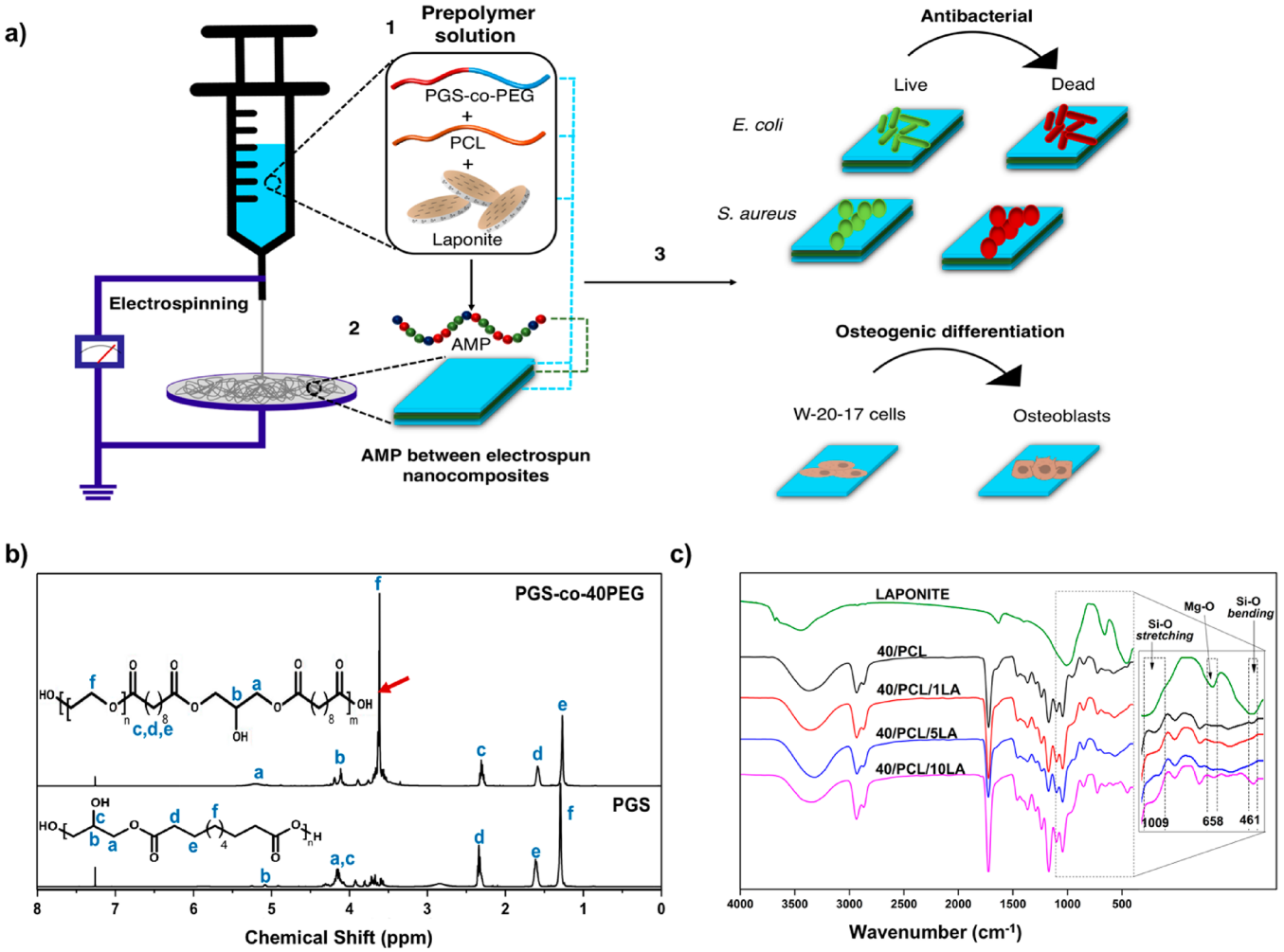

Figure 1. Fabrication process and chemical characterization of the nanocomposites. (a) Schematic of the fabrication process of the nanocomposites: 1 refers to the prepolymer solution containing PGS-*co*-PEG, PCL, and Laponite used in the scaffolds fabrication process, 2 refers to the addition of AMP during the electrospinning process in between the scaffolds' layers, and 3 refers to the resulting scaffolds were tested for the antibacterial effect and their ability to enhance the osteogenic differentiation of cells. (b) ^{1}H NMR spectra of PGS and PGS-*co*-40PEG, indicating the additional methylene peak (referred to by the red arrow) in the PGS-*co*-40PEG spectrum confirming the presence of PEG. (c) FTIR spectra of Laponite, 40/PCL/1LA, 40/PCL/5LA, 40/PCL/10LA showing the characteristic bands of Laponite within the nanocomposites.

min at room temperature on a shaker. Two microliters of pNPP, 200 μL of assay buffer, and 5 μL of Mg acetate were added to 50 μL of the cell lysates. The same amount of the reagents was added to 50 μL ultrapure H_2O as a blank. A microplate reader (Bio-Tek Inc.) was used to measure the absorbance at 405 nm, and the ALP activity was calculated from a standard calibration curve and according to the manufacturer's procedure ($n \geq 3$).

2.5.7. RNA Isolation and Real Time PCR (RT-PCR). RNA was isolated from cells seeded on 40/PCL and 40/PCL/5LA samples using TRIzol (Invitrogen) at day 7 post culture. The concentration of RNA was determined using a NanoDrop 2000/2000c Spectrophotometer at 260 and 280 nm. cDNA was synthesized using random-hexamer primers and RNase free reverse transcriptase (Roche first strand cDNA synthesis kit) in a total volume reaction of 20 μL for 45 min (10 min at 25 °C, then 30 min at 55 °C, followed by incubation at 85 °C for 5 min, and finally held at 4 °C). Gene expression quantification was performed using a TAQMAN Mater mix (ThermoFisher scientific), Taqman primers, and cDNA synthesized in the previous step ($n \geq 3$). Genes and their respective primer sequences are listed in Table S3.

2.6. Release Profile of AMP (Tet213). The in vitro cumulative release profile of AMP from the 0.2AMP and 0.4AMP nanocomposites was obtained using a microplate reader (Bio-Tek, Inc.). Accordingly, the scaffolds were incubated in 2 mL of DPBS at 37 °C in an incubator shaker. At specific time points, 100 μL of solution was removed, and the solutions were replenished with fresh DPBS. The absorbance of AMP solutions was recorded at 280 nm, which corresponded to the absorption peak characteristic for tryptophan in AMP. Scaffolds without AMP were used as blanks to eliminate any interference. Series of dilutions of the AMP in DPBS ranging from 25 to 100 μg/mL were prepared to obtain the standard curve ($n \geq 3$).

2.7. Antimicrobial Activity Evaluation. Antimicrobial activity of 0.2AMP and 0.4AMP nanocomposites were examined against Gram-positive (*S. aureus*) (ATCC 12600) and Gram-negative (*E. coli*) (ATCC 25922) bacteria and compared to 40/PCL/5LA samples with no AMP, which served as controls. Single colonies of each bacterial strain were incubated overnight in a shaking incubator (200 rpm at 37 °C). After it was mixed with tryptic soy broth (TSB; Bacto; 5 mL), the concentration of the bacterial solutions was adapted to an optical density (OD) value of 0.52 at 562 nm (representing 10^9 CFU/mL) using a microplate reader (SpectraMax Paradigm). Next, the bacterial suspensions were diluted to 10^6 CFU/mL. The scaffolds were sterilized by UV for 30 min before being placed in 24 well plates with 1 mL bacterial solution (10^6 CFU/mL). The samples were then incubated for 6 or 12 h at 37 °C and 5% CO_2. Next, the ODs were recorded using a microplate reader (SpectraMax Paradigm) at 562 nm. For the colony forming units (CFU) test, incubated samples were removed after 12 h and washed three times with DPBS. The scaffolds

https://dx.doi.org/10.1021/acsabm.0c00250
ACS Appl. Bio Mater. 2020, 3, 3313−3325

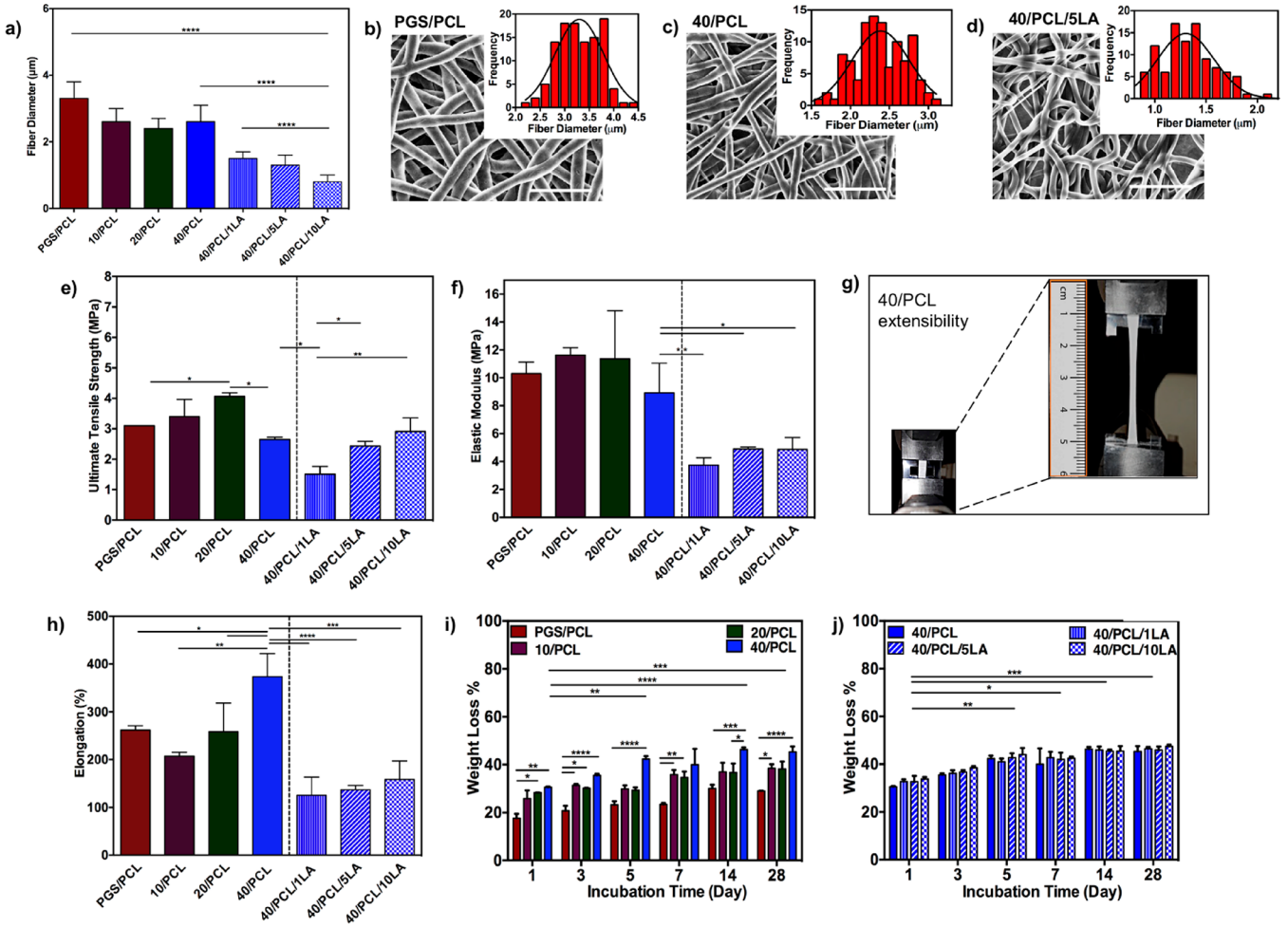

Figure 2. Physical characterization of the nanocomposites. (a) Average fiber diameter for different nanocomposite formulations. Representative SEM images for (b) PGS/PCL, (c) 40/PCL, and (d) 40/PCL/5LA, respectively, with fiber diameter distribution (scale bar = 10 μm). (e) Ultimate tensile strength and (f) elastic modulus for different nanocomposite formulations. (g) Representative image from the uniaxial mechanical testing demonstrating the high extensibility of 40/PCL scaffolds. (h) Elongation of scaffolds with various formulations. (i) In vitro degradation of PGS/PCL and PGS-*co*-PEG/PCL scaffolds. (j) Effect of Laponite addition on the in vitro degradation profile of the nanocomposites. Data are represented as mean ± SD ($*p < 0.05$, $**p < 0.01$, $***p < 0.001$, $****p < 0.0001$, ($n \geq 3$))

were then placed in 1 mL microcentrifuge tubes and vortexed at 3000 rpm for 15 min to release the bacteria from the scaffolds into the solution. The resulting bacterial solutions were serially diluted with DPBS in 96-well plates over 4 logarithmic dilutions. From each dilution, 10 μL of the bacterial solutions were seeded on tryptic soy agar plates and incubated for 24 h at 37 °C and 5% CO_2. Finally, the bacterial colonies number on each agar plate were counted and reported as CFU. For SEM imaging, the samples were incubated with 10^6 CFU/mL for 12 h and washed three times with DPBS, followed by fixation in 4% paraformaldehyde for 15 min. The scaffolds were, then, dehydrated with serial dilutions of ethanol (30%, 50%, 70%, and 100%) and, finally, freeze-dried overnight. After samples were sputter coated with gold at 20 mA for 2 min, SEM images (ZEISS Leo Supra55 field emission SEM) were obtained at an accelerating voltage of 8 kV (LADD Hummer 8 Sputter Coater) ($n \geq 3$).

2.8. Statistical Analysis. The analysis of the data was performed through a Student's *t* test or one-way ANOVA using GraphPad Prism 6.0 software. Error bars presented the mean ± standard deviation (SD) of measurements ($*p < 0.05$, $**p < 0.01$, $***p < 0.001$, and $****p < 0.0001$).

3. RESULTS AND DISCUSSION

In this study, we engineered elastomeric electrospun nanocomposites based on highly elastic copolymer PGS-*co*-PEG with osteoinductive and antimicrobial properties. Recent studies have shown the remarkable effect of matrix elasticity on bone tissue regeneration.[16,17] This is mainly because elastic scaffolds are able to transduce the applied load to the recruited progenitor cells guiding their differentiation, matrix maturation, and bone remodeling in vivo and in vitro.[16,17] Therefore, we developed a highly elastic PGS-*co*-PEG fibrous scaffold for bone tissue engineering applications. To enhance the osteoinductive properties of the scaffold, we incorporated Laponite nanosilicates within the polymer matrix. In addition, to impart antimicrobial properties, we incorporated an AMP within the nanocomposites. Physical characterizations were performed to evaluate morphology, mechanical characteristics, and degradability of the nanocomposites. The antimicrobial activity of the nanocomposites was examined against *E. coli* and *S. aureus* as models for Gram-negative and Gram-positive bacteria, respectively. Finally, the optimized nanocomposites were used to assess in vitro osteogenic differentiation of W-20-17 pre-osteoblasts to assess the suitability of the engineered materials for bone tissue regeneration (Figure 1a).

3.1. Synthesis and Chemical Characterization of PGS-*co*-PEG and Nanocomposite Scaffolds. PGS-*co*-PEG

https://dx.doi.org/10.1021/acsabm.0c00250
ACS Appl. Bio Mater. 2020, 3, 3313−3325

prepolymers were synthesized by varying the glycerol/PEG molar ratio in a two-step polycondensation reaction.[15] The molecular weights determined by GPC were 4483, 6572, 6346, and 7331 g/mol for PGS, PGS-*co*-10PEG, PGS-*co*-20PEG, and PGS-*co*-40PEG, respectively. ^{1}H NMR analysis confirmed the successful synthesis of PGS-*co*-PEG copolymers (Figure 1b). The ^{1}H NMR spectrum of PGS showed three peaks attributed to methylene groups at 1.3, 1.6, and 2.3 ppm. In addition, peaks indicative of the protons in glycerol were visible at 4.1 and 5.2 ppm. An additional methylene peak was observed at 3.6 ppm in the ^{1}H NMR spectrum of PGS-*co*-40PEG, confirming the presence of PEG in the copolymer backbone.[15] As demonstrated in Table S1, the PEG percentage within PGS-*co*-10PEG, PGS-*co*-20PEG, and PGS-*co*-40PEG was calculated from the integration of methylene peaks of PEG and sebacic acid. A close correlation between the theoretical PEG ratio and the ratio calculated from ^{1}H NMR was found, indicating precise control over the copolymer synthesis reaction.

FTIR analysis (Figure S1a) further confirmed the presence of PEG and PGS in the backbone of the PGS-*co*-PEG copolymers, where both PGS and PGS-*co*-PEG showed similar overlapping peaks with different intensities at different PEG concentration. A typical absorption peak assigned to the stretching vibration of (C═O) at 1725 cm^{-1} validated the presence of PGS in the copolymer. In addition, a broad absorption peak characteristic of an (O−H) group was observed at 3360 cm^{-1}, and another two absorption peaks for (C−H) bonds were observed at 2927.8 and 2865.7 cm^{-1} for the asymmetrical and symmetrical stretching vibrations, respectively. Furthermore, two absorption peaks assigned for (C−C) vibration modes and symmetrical stretching vibrations of (C−O−C) were observed in the range from 1100 to 1400 cm^{-1}.[15,25,26] FTIR analyses of PCL, PGS, 10/PCL, 20/PCL, and 40/PCL are shown in Figure S1b. The PCL spectrum showed two main absorption bands at 1241 and 1291 cm^{-1} related to the asymmetric stretching of (C−O−C), (C−O), and (C−C), respectively. Similar bands were observed for the electrospun PGS/PCL, 10/PC, 20/PC, and 40/PCL, indicating the presence of PCL. Other absorption bands were visible around 1725 cm^{-1}, representative of carbonyl stretching[25,27] and was characteristic of PGS and all PGS-*co*-PEG copolymers.

To impart osteoinductive properties to the fabricated electrospun scaffolds, different concentrations of Laponite nanosilicates known for inducing osteogenesis,[28,29] were added to 40/PCL (PGS-*co*-40PEG) samples. Laponite integration within 40/PCL scaffolds was confirmed by FTIR analysis (Figure 1c), indicating three typical absorption bands at 461 cm^{-1} (attributed to Si−O bending mode), at 658 cm^{-1} (Mg−O bonding), and a broad absorption band at 1009 cm^{-1} (Si−O stretching mode).[30−32] The same three characteristic absorption peaks were observed in other samples with enhanced intensity as the concentration of Laponite increased, indicating the successful incorporation of the Laponite within the 40/PCL scaffolds.

3.2. Physical Characterization of the Scaffolds. The physical properties of the engineered scaffolds were characterized for their morphology, mechanical properties, and degradation profile. The 40/PCL samples were used to be loaded with Laponite and AMP because of its desired mechanical properties. They were used to study the effect of the addition of these components on the physical properties of the resulting scaffolds. The average fiber diameters of PGS/PCL, 10/PCL (PGS-*co*-10PEG/PCL), 20/PCL (PGS-*co*-20PEG/PCL), and 40/PCL (PGS-*co*-40PEG/PCL) were 3.3 ± 0.5, 2.6 ± 0.4, 2.4 ± 0.3, and 2.6 ± 0.5 μm, respectively. The incorporation of Laponite within the 40/PCL scaffolds decreased the average fiber diameter to 1.5 ± 0.2 μm for 40/PCL/1LA, 1.3 ± 0.3 μm for 40/PCL/5LA, and 0.8 ± 0.2 μm for 40/PCL/10LA (Figure 2a), which is in agreement with previous reports.[33,34] However, this reduction in average fiber diameter did not have a significant influence on the average pore size of scaffolds composed of different polymers and different Laponite concentrations (40/PCL/1LA, 40/PCL/5LA, and 40/PCL/10LA, Table S2). The morphological analysis of the scaffolds by SEM showed smooth, non-beaded fibers for scaffold with different formulations. Additionally, the morphology did not change after the incorporation of Laponite as shown in Figures 2b−d and S2.

Mechanical properties are important in determining the scaffolds suitability for bone tissue engineering. In this regard, the mechanical properties of the scaffolds were assessed. The results revealed a drop in the ultimate tensile stress (UTS) for 40/PCL (2.65 ± 0.1 MPa) as compared to PGS/PCL (3.1 MPa), which could be due to the increase in PEG content.[15] However, no significant changes were observed in the UTS values for 10/PCL and 20/PCL in comparison to PGS/PCL (Figure 2e). This can be mainly due to lack of enough PEG content within 10/PCL and 20/PCL scaffolds, which could not illicit distinguished mechanical properties as compared to PGS/PCL samples. Furthermore, the addition of Laponite negatively affected the UTS values for the composite containing 1% Laponite, (decreased from 2.65 ± 0.1 to 1.5 ± 0.25 MPa for 40/PCL and 40/PCL/1LA, respectively) (Figure 2e). However, there was no significant differences in UTS values of 40/PCL/5LA, 40/PCL/10LA, and 40/PCL.

On the basis of the tensile test, the PGS/PCL, 10/PCL, 20/PCL, and 40/PCL scaffolds showed an elastic modulus within the range of 9−11 MPa. The addition of 1%, 5%, and 10% Laponite into 40/PCL led to a dramatic drop in the elastic modulus compared to pure 40/PCL sample (Figure 2f). In addition, the 40/PCL scaffold exhibited the highest elongation with a ∼2-fold increase as compared to PGS/PCL (Figure 2g and h). There was no significant difference between the elongation values of PGS/PCL, 10/PCL, and 20/PCL, although the elongation of these scaffolds was comparatively lower than 40/PCL scaffold (almost ∼2-fold lower). The higher extensibility of 40/PCL scaffold can be attributed to the high PEG content, leading to a more elastic scaffold.[15,35] The elongation showed a significant decrease upon addition of Laponite (Figure 2g and h). A similar drop in mechanical properties was reported previously in Laponite containing nanocomposites.[33,36] It was a result of a decrease in the fiber diameter, which led to more brittle fibers and consequently less elongation.[33,36] Another factor that might have contributed to the decrease in the mechanical properties is the possibility that Laponite might be aggregated within the electrospun fibers eventually affecting the elastic deformation within the nanocomposites.[33]

Elastic scaffolds have become advantageous for bone regeneration.[16,37] The elastic structures of such scaffolds provide a load-transducing environment. This potentially facilitates the ECM deposition, formation, and maturation of new bone.[16] Since 40/PCL showed the highest elasticity of almost 400%, we used this formulation to form composite scaffolds with Laponite.

https://dx.doi.org/10.1021/acsabm.0c00250
ACS Appl. Bio Mater. 2020, 3, 3313−3325

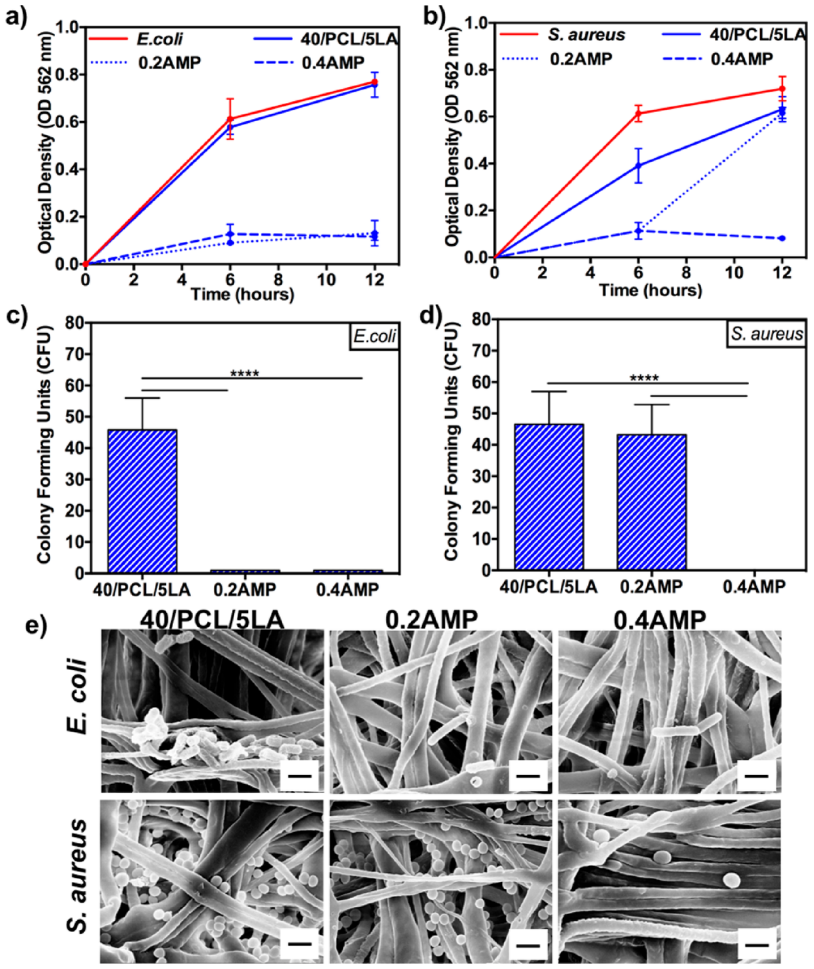

Figure 3. Antimicrobial activity of the nanocomposites loaded with AMP (0.2AMP and 0.4AMP). (a, b) Optical density (OD) of 0.2AMP and 0.4AMP nanocomposites after 6 and 12 h incubation with Gram-negative *E. coli* and Gram-positive *S. aureus*. (c, d) Colony forming unit (CFU) test showing the effect of 0.2AMP and 0.4AMP nanocomposites after 12 h against Gram-negative *E. coli* and Gram-positive *S. aureus*. (e) Representative SEM images of nanocomposites with and without AMP showing their influence on bacteria growth for both *E. coli* and *S. aureus* (scale bar = 2 μm). Data are represented as mean ± SD (****$p < 0.0001$, ($n \geq 3$)).

Despite the decrease in mechanical properties after addition of Laponite, the properties of the nanocomposites were still within the suitable range for bone tissue engineering (e.g., elastic modulus up to 5 MPa and elongation of 100%).[33] Therefore, we selected 40/PCL/5LA as a model for further biological evaluation due to its higher mechanical properties as compared to 40/PCL/1LA. In addition, 40/PCL/5LA had less Laponite agglomeration compared to 40/PCL/10LA, making it more suitable for the electrospinning process.

These nanocomposites were further modified with AMP to provide antimicrobial characteristics. We evaluated the effect of AMP on the mechanical properties of the nanocomposite and found that the addition of AMP had no effect on the mechanical properties of the resulting scaffolds (Figure S3a–c). This is in consistence with recent studies from our group, which showed that the integration of AMP within a hydrogel matrix did not affect the mechanical properties of the hydrogel.[38,39] This was due to the small size of AMP, which subsequently could not change the polymeric network microstructure and stiffness.[39]

It is well established that the degradation of PCL occurs through either surface or bulk degradation through two steps hydrolytic cleavage of ester groups and intracellular polymer digestion facilitated through giant cells, macrophages, and fibroblasts at low polymer molecular weights.[40] On the other hand, PGS-*co*-PEG degrades via surface erosion, where the degradation rate increases with increasing PEG concentration. The PEG content enhances the hydrophilicity of the copolymer, which accelerates the hydrolysis of the PGS.[15,41] Unlike PCL, which has a slow degradation rate (up to several years), PGS-*co*-PEG has a relatively fast degradation rate that can occur in days to months. Moreover, Laponite also has a hydrophilic nature.[42] Taking all this together, it is anticipated that the degradation rate of the scaffolds can be tuned through three factors: altering PCL/PGS-*co*-PEG ratio, controlling the PEG ratio within the PGS-*co*-PEG copolymer, and adjusting the Laponite concentration within the nanocomposites. This enables us to fabricate scaffolds for bone tissue engineering with tunable degradation rates for both small or large bone defects.[33,43]

The degradation profile of the scaffolds with various formulations was evaluated by incubating samples in DPBS at 37 °C and measuring weight loss over 28 days. The results showed that the degradation rate increased with increasing the PEG content (Figure 2i). For example, after 28 days, 10/PCL, 20/PCL, and 40/PCL scaffolds showed 38.5 ± 1.6, 38.3 ± 3, and 45.4 ± 2.2% weight loss, respectively, which was comparatively higher than PGS/PCL (29 ± 0.7%). Further-

https://dx.doi.org/10.1021/acsabm.0c00250
ACS Appl. Bio Mater. 2020, 3, 3313–3325

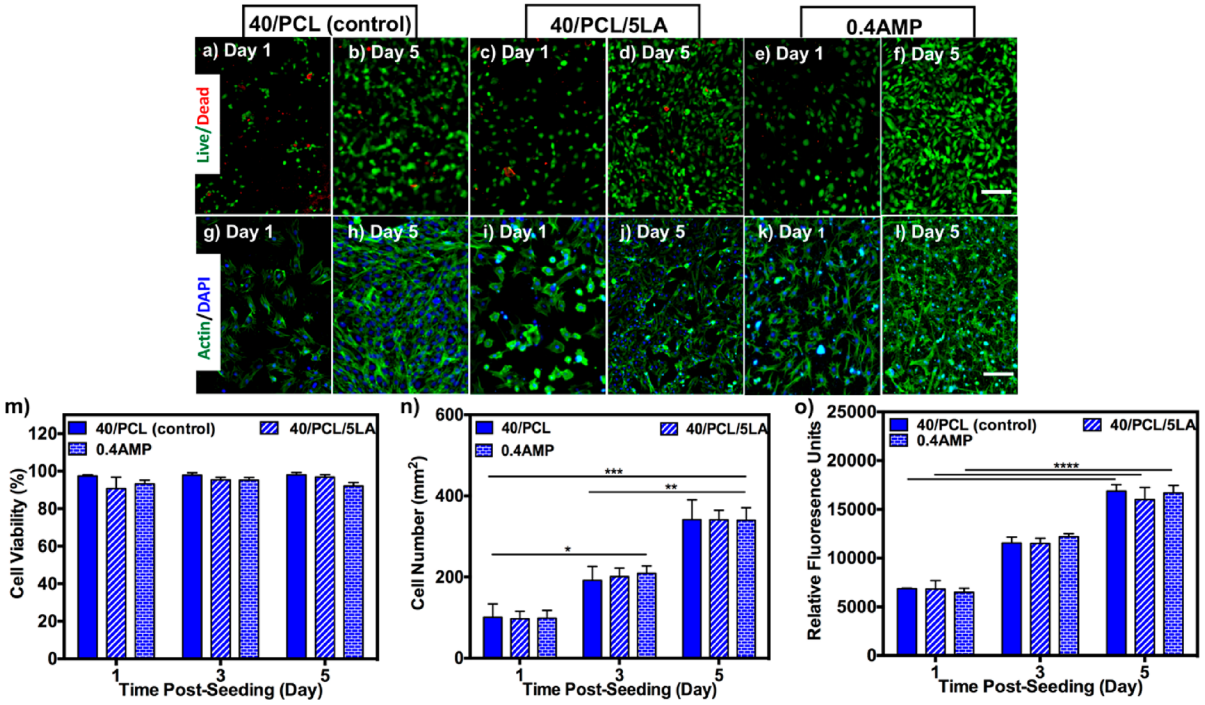

Figure 4. In vitro cytocompatibility of the nanocomposites. (a–f) Representative live/dead images of W-20-17 cells cultured on 40/PCL, 40/PCL/5LA, and 0.4AMP at days 1 and 5 (scale bar = 100 μm). (g–l) Representative Actin/DAPI images of W-20-17 cells cultured on 40/PCL, 40/PCL/5LA, and 0.4AMP after 1 and 5 days (scale bar = 100 μm). (m) Quantification of cell viability for cells cultured on 40/PCL, 40/PCL/5LA, and 0.4AMP after 1, 3, and 5 days of seeding. (n) Quantification of the number of cells per unit area for the cells cultured on 40/PCL, 40/PCL/5LA, and 0.4AMP at day 1, 3, and 5 post seeding. (o) Metabolic activity of W-20-17 cells cultured on 40/PCL, 40/PCL/5LA, and 0.4AMP after 1, 3, and 5 days. Data are represented as mean ± SD ($*p < 0.05$, $**p < 0.01$, $***p < 0.001$, $****p < 0.0001$, ($n \geq 3$)).

more, the addition of Laponite did not have a significant effect on the degradation rate (Figure 2j). For example, 40/PCL/1LA, 40/PCL/5LA, and 40/PCL/10LA scaffolds had a weight loss of 49 ± 1.4%, 50.5 ± 0.7%, and 56.8 ± 0.3%, respectively, after 28 days. This slight enhancement in hydrophilicity might be due to the decrease in the average fiber diameter of nanocomposites, which may facilitate DPBS diffusion and promote the hydrolysis of both PCL and PGS-*co*-40PCL.[33]

3.3. Antimicrobial Properties of Nanocomposites Loaded with AMP. The risk of bacterial infection associated with orthopedic implants and bone graft materials can lead to the implant failure.[11,44] Thus, it is desirable to design scaffolds that are not only biocompatible, osteoinductive, and mechanically stable but also possess antimicrobial properties to hinder bacterial colonization. AMP is effective against both Gram-negative and Gram-positive bacteria, including drug resistant strains.[45,46] This function depends on their ability to disrupt the bacterial membrane through electrostatic interactions because of the negative charge on bacteria surfaces.[46] In addition, AMP has been used as potent antimicrobial agents for implant coatings or bone cements without any negative effect on bone formation process.[47−49] As such, the incorporation of AMP within 40/PCL/5LA nanocomposite should provide the scaffold with antimicrobial properties, without inhibiting its osteoinductive properties.

First, the release profile of AMP from 0.2AMP and 0.4AMP nanocomposites was investigated. 0.2AMP and 0.4AMP nanocomposites were prepared through adding 0.2% or 0.4% (w/v) AMP solutions on top of each layer of 40/PCL/5LA during the electrospinning process. Next, 0.2AMP and 0.4AMP nanocomposites were incubated in DPBS at 37 °C, and the cumulative release of AMP was measured at an absorption wavelength of 280 nm. 40/PCL/5LA scaffold without AMP was used as control. A burst release of the AMP was observed within the first hour, followed by complete release of AMP after 4 h (Figure S3d). This can be explained due to the physical entrapment and absence of chemical bonding between AMP molecules and polymer backbone in the nanocomposite. For sustained release, further investigation should focus on the encapsulation of AMP within the fibers of the nanocomposite, within nanocarriers, or immobilization on Laponite nanoplates, for the long-term release since ideally a high dose of antimicrobial agents is required for the first 1−2 days post-implantation.[34,50,51]

The antimicrobial activity of the AMP-loaded nanocomposites was then evaluated against both Gram-negative (*E. coli*), and Gram-positive (*S. aureus*) bacteria, which can cause orthopedic implant failure.[52] Antimicrobial activity was determined by measuring optical density (OD) and performing a CFU assay. For optical density measurement, four groups were used: bacteria solutions, 40/PCL/5LA, 0.2AMP, and 0.4AMP nanocomposites. OD was measured for bacteria solutions (10^6 CFU/mL) in tryptic soy broth (TSB) media. The results showed a significant reduction in the bacteria growth curve for both *E. coli* and *S. aureus* with nanocomposites containing AMP (0.2AMP and 0.4AMP) as compared to the samples without AMP or the bacteria solution after 6 h incubation. The reduction in the growth, as observed by the OD reading, was continued after 12 h for *E. coli* for both 0.2AMP and 0.4AMP nanocomposites (Figure 3a). However, for *S. aureus*, the antimicrobial effect was prevalent only with 0.4AMP nanocomposite (Figure 3b). These results were confirmed by CFU assay using 40/PCL/5LA, 0.2AMP, and 0.4AMP nanocomposites. The results

https://dx.doi.org/10.1021/acsabm.0c00250
ACS Appl. Bio Mater. 2020, 3, 3313−3325

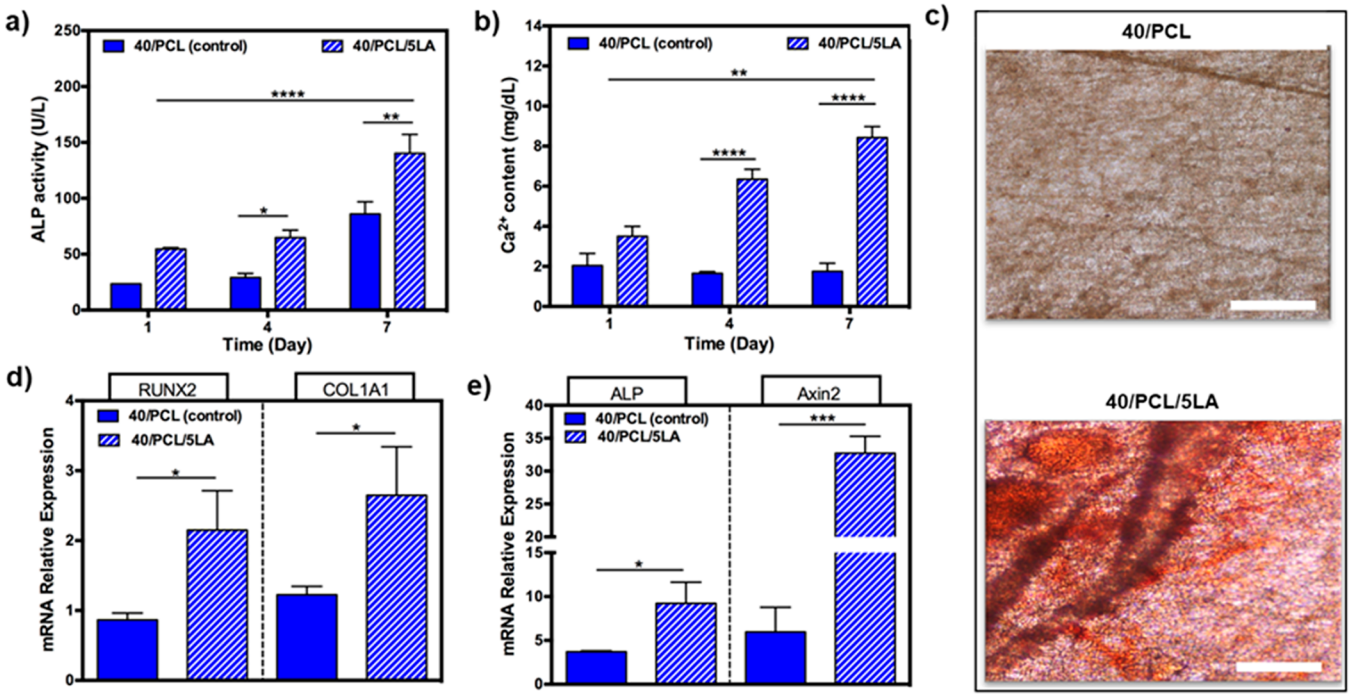

Figure 5. Effect of Laponite-containing nanocomposites on osteogenic differentiation of cells. (a) Alkaline phosphatase (ALP) activity after 1, 4, and 7 days of cell seeding on 40/PCL and 40/PCL/5LA. (b) Quantification for the Ca^{2+} deposited by cells cultured on 40/PCL and 40/PCL/5LA scaffolds after 1, 4, and 7 days. (c) Alizarin red staining of the mineralized matrix deposition by cells cultured on 40/PCL and 40/PCL/5LA on day 7 post seeding (scale bar = 200 μm). (d, e) RT-PCR analysis evaluating the relative expression of mRNA of the osteogenic markers RUNX2, ALP, Axin2, and the extracellular matrix deposition marker, COL1A1. Data are represented as mean ± SD (*p < 0.05, **p < 0.01, ***p < 0.001, ****p < 0.0001, ($n \geq 3$)).

indicated that 0.2AMP and 0.4AMP nanocomposites could effectively inhibit the growth of *E. coli* when compared to 40/PCL/5LA (Figure 3c). However, for *S. aureus*, only the 0.4AMP sample was effective (Figure 3d). SEM images for nanocomposites incubated in TSB with 10^6 CFU/mL of *E. coli* or *S. aureus* supported the results from OD reading and CFU assay. As shown in Figure 3e, 0.2AMP and 0.4AMP were highly effective against *E. coli* in comparison to 40/PCL/5LA. In contrast, only 0.4AMP demonstrated significant antimicrobial properties against *S. aureus* when compared to 40/PCL/5LA and 0.2AMP. This prominent effect of 0.4AMP nanocomposite against Gram-negative *E. coli* may be due to the more negative charge of *E. coli*'s surface combined with the fact that AMP has higher affinity for negatively charged surfaces. This could attract more AMP to *E. coli* compared to *S. aureus*, leading to a stronger antibacterial activity of AMP at lower concentrations.[53,54] Also, the differences in Gram-negative versus Gram-positive bacteria, particularly their proteoglycan layers, could have played a major role. Since Gram-negative bacteria have thinner proteoglycan layers, this may have facilitated the permeability of AMP at lower concentrations.[55] Consequently, AMP was effective against *S. aureus* only at higher concentration. Similar results were reported by Bhowmick et al., where they found that magnetic nanocomposites containing nanohydroxyapatite−Fe_3O_4 were more effective toward Gram-negative bacteria as a result of the low thickness of proteoglycan layers compared to Gram-positive bacteria.[11] It is noteworthy to mention that the presence of Laponite did not alter the antimicrobial properties of the nanocomposites, which is in agreement with previous reports.[49] Moreover, it has been suggested that AMP-loaded nanocomposites may be more effective in vivo because of an expected lower number of bacterial colonies.[56]

3.4. Biocompatibility of the Nanocomposites. The biocompatibility of the nanocomposites was assessed by seeding W-20-17 on the surface of 40/PCL, 40/PCL/5LA and 0.4AMP. Cell viability was evaluated using a live/dead kit on days 1 and 5 post-seeding. The results showed that cells cultured on all tested nanocomposites maintained more than 90% viability (Figure 4a−f and m), confirming the in vitro cytocompatibility of the engineered scaffolds. Furthermore, the addition of Laponite and AMP did not show any negative effect on cytocompatibility, which is in agreement with previous reports.[40,48] Actin/DAPI staining was used to stain F-actin filaments and nuclei to evaluate the ability of nanocomposites to support spreading and proliferation of cells. The quantification of cell density on the surface of the scaffolds revealed high cell spreading and proliferation after 5 days of culture (Figure 4g−l). Additionally, cell nuclei per unit area was measured, which showed an increase over time with a ∼3.5-fold enhancement after day 5 postseeding (Figure 4n). Moreover, PrestoBlue assay was used to evaluate the metabolic activity of the cells. The cells showed a constant increase in the metabolic activity with no significant change between the tested groups (Figure 4o).

3.5. Osteogenic Activity of Nanocomposites. The osteogenic differentiation of the W-20-17 cells seeded on the surface of engineered scaffolds was investigated through evaluating the ALP activity, mineralized matrix deposition, and the expression levels of the osteogenesis markers using RT-PCR analysis. W-20-17 cells are murine pre-osteoblast bone marrow stromal cells that are capable of differentiating into osteoblasts when cultured on osteoinductive surfaces and

https://dx.doi.org/10.1021/acsabm.0c00250
ACS Appl. Bio Mater. 2020, 3, 3313−3325

in the presence of bone morphogenetic protein 2 (BMP-2).[57−60] Alkaline phosphatase (ALP) was used as an early indicator for osteoblastic differentiation and mineralization.[60] W-20-17 cells were seeded on 40/PCL (control) and 40/PCL/5LA scaffolds, and ALP activity was investigated at days 1, 4, and 7. Cells seeded on 40/PCL/5LA showed a significant enhancement in ALP at days 4 and 7 as compared to 40/PCL scaffolds without Laponite (Figure 5a). Similarly, a previous study reported that the level of ALP increased in the presence of BMP-2 after 7 days for a W-20-17 cell seeded chitosan gel.[61]

In addition to ALP, calcium deposition and alizarin red staining were used to detect the degree of mineralization produced by cells seeded on 40/PCL/5LA and 40/PCL nanocomposites. A considerable elevation in calcium levels was observed in the cells seeded on 40/PCL/5LA when compared to 40/PCL after 4 and 7 days of seeding (Figure 5b). After 7 days in culture, the nanocomposites were stained with alizarin red, which indicated an enhancement in the mineralized matrix formation depicted by the red color shown on 40/PCL/5LA nanocomposites (Figure 5c).

We further investigated the expression levels of the early osteogenic markers runt-related transcription factor 2 (RUNX2), ALP, collagen type 1 alpha 1 (COL1A1), which are responsible for the synthesis of ECM, and Axin2, a regulator of Wnt signaling pathways that plays a vital role in osteogenic differentiation.[62,63] The upregulation of these markers is associated with enhanced osteoblastic activity. Compared to cells cultured on 40/PCL, W-20-17 cells seeded on 40/PCL/5LA showed a ∼2-fold enhancement in the expression level of RUNX2 and COL1A1 (Figure 5d). Similarly, ALP and Axin2 exhibited prominent upregulation level in cells cultured on 40/PCL/5LA (Figure 5e). Similar behavior was observed in Laponite incorporated polymeric matrices in previous studies. For example, poly(ethylene oxide) (PEO) hydrogels containing Laponite showed a 2-fold enhancement in mineralized matrix deposition by MC3T3 cells when compared to cells cultured on tissue culture polystyrene (TCPS) (positive control).[64] In another study, nanocomposite hydrogels composed of gelatin methacryloyl (GelMA) and Laponite demonstrated the ability of Laponite to trigger the osteogenic differentiation of human mesenchymal stem cells (hMSCs) through an elevation in ALP activity and the degree of mineralization when compared to GelMA without Laponite.[28] In addition, the inclusion of Laponite in a catechol-modified gelatin methacryloyl (GelMA-DOPA) as an adhesive hydrogel matrix upregulated early markers involved in the osteogenic differentiation.[49] These results from other reports are consistent with the results presented here, indicating the potential of 40/PCL/5LA nanocomposites to be used as osteoinductive substrates that support osteogenic differentiation.

4. CONCLUSION

In this study, we report on the fabrication and characterization of elastic PGS-*co*-PEG based nanocomposites with dual osteoinductive and antimicrobial properties for bone regeneration. The scaffolds were fabricated from the highly elastic PGS-*co*-PEG and PCL polymers with the addition of Laponite nanosilicates and AMP to provide osteoinductive and antimicrobial characteristics, respectively. Chemical characterization using ^{1}HNMR and FTIR validated the successful synthesis of PGS-*co*-PEG polymers and the presence of Laponite within the electrospun scaffolds. The addition of Laponite to the electrospun scaffolds led to a decrease in fiber diameter and mechanical properties. Nevertheless, scaffolds were still within the acceptable range used in bone tissue engineering. Also, an increase in the degradation rate was observed after the addition of Laponite. Introducing the AMP provided antimicrobial properties against both Gram-negative *E. coli* and Gram-positive *S. aureus* bacteria. Furthermore, 2D culture of W-20-17 cells on the surface of the nanocomposites showed high viability and enhanced proliferation and metabolic activity, indicating the biocompatibility of these nanocomposites. The ability of the nanocomposites to support the osteogenic differentiation was also assessed using W-20-17 cells. The incorporation of Laponite led to enhanced ALP activity and mineralization. Moreover, it showed an upregulation of markers related to osteogenic differentiation. Overall, the results presented in this study suggest the suitability of PGS-*co*-PEG based nanocomposites as potential platforms for bone tissue engineering. Such applications require multifunctional properties including osteoinductivity and antimicrobial activity, which were demonstrated in the reported nanocomposites. Our future study will focus on the in vivo validation of the osteoinductive potential of the engineered nanocomposites.

■ ASSOCIATED CONTENT

Supporting Information

The Supporting Information is available free of charge at https://pubs.acs.org/doi/10.1021/acsabm.0c00250.

FTIR spectra of PGS, PGS-*co*-10PEG, PGS-*co*-20PEG, PGS-*co*-40PEG, PCL, 10/PCL, 20/PCL, and 40/PCL; representative SEM images for 10/PCL, 20/PCL, 40/PCL/1LA, and 40/PCL/10LA; AMP effect on the nanocomposites mechanics and AMP release; tryptic soy agar plates for CFU test; NMR ratio between PGS and PEG; summary for average fiber diameter sand pore sizes of different scaffolds; and RT-PCR primer sequences (PDF)

■ AUTHOR INFORMATION

Corresponding Author

Nasim Annabi − *Department of Chemical and Biomolecular Engineering and Center for Minimally Invasive Therapeutics (C-MIT), California NanoSystems Institute (CNSI), University of California—Los Angeles, Los Angeles, California 90095, United States;* orcid.org/0000-0003-1879-1202; Phone: +1(310) 267-5927; Email: nannabi@UCLA.edu

Authors

Dina M. Ibrahim − *Energy Materials Laboratory (EML), School of Sciences and Engineering, The American University in Cairo, New Cairo 11835, Egypt; Department of Chemical Engineering, Northeastern University, Boston, Massachusetts 02115, United States*

Ehsan Shirzaei Sani − *Department of Chemical and Biomolecular Engineering, University of California—Los Angeles, Los Angeles, California 90095, United States*

Alaa M. Soliman − *Energy Materials Laboratory (EML), School of Sciences and Engineering, The American University in Cairo, New Cairo 11835, Egypt*

Nooshin Zandi − *Department of Chemical Engineering, Northeastern University, Boston, Massachusetts 02115, United*

https://dx.doi.org/10.1021/acsabm.0c00250
ACS Appl. Bio Mater. 2020, 3, 3313−3325

States

Ebrahim Mostafavi − *Department of Chemical Engineering, Northeastern University, Boston, Massachusetts 02115, United States;* orcid.org/0000-0003-3958-5002

Ahmed M. Youssef − *Packaging Materials Department, National Research Centre, Giza 12622, Egypt*

Nageh K. Allam − *Energy Materials Laboratory (EML), School of Sciences and Engineering, The American University in Cairo, New Cairo 11835, Egypt*

Complete contact information is available at: https://pubs.acs.org/10.1021/acsabm.0c00250

Notes

The authors declare no competing financial interest.

■ ACKNOWLEDGMENTS

N.A. acknowledges the financial support from the National Institutes of Health (NIH) (R01EB023052; R01HL140618). D.M.I. acknowledges the travel abroad grant provided by the American University in Cairo, Egypt.

■ REFERENCES

(1) De Witte, T.-M.; Fratila-Apachitei, L. E.; Zadpoor, A. A.; Peppas, N. A. Bone Tissue Engineering via Growth Factor Delivery: From Scaffolds to Complex Matrices. *Regen. Biomater.* **2018**, *5*, 197−211.

(2) Porter, J. R.; Ruckh, T. T.; Popat, K. C. Bone Tissue Engineering: A Review in Bone Biomimetics and Drug Delivery Strategies. *Biotechnol. Prog.* **2009**, NA−NA.

(3) Amini, A. R.; Laurencin, C. T.; Nukavarapu, S. P. Bone Tissue Engineering: Recent Advances and Challenges. *Crit. Rev. Biomed. Eng.* **2012**, *40* (5), 363−408.

(4) Nasajpour, A.; Ansari, S.; Rinoldi, C.; Rad, A. S.; Aghaloo, T.; Shin, S. R.; Mishra, Y. K.; Adelung, R.; Swieszkowski, W.; Annabi, N.; Khademhosseini, A.; Moshaverinia, A.; Tamayol, A. A Multifunctional Polymeric Periodontal Membrane with Osteogenic and Antibacterial Characteristics. *Adv. Funct. Mater.* **2018**, *28*, 1703437.

(5) El-Rashidy, A. A.; Roether, J. A.; Harhaus, L.; Kneser, U.; Boccaccini, A. R. Regenerating Bone with Bioactive Glass Scaffolds: A Review of in Vivo Studies in Bone Defect Models. *Acta Biomater.* **2017**, *62*, 1−28.

(6) Holmes, B.; Castro, N. J.; Zhang, L. G.; Zussman, E. Electrospun Fibrous Scaffolds for Bone and Cartilage Tissue Generation: Recent Progress and Future Developments. *Tissue Eng., Part B* **2012**, *18* (6), 478−486.

(7) Zandi, N.; Lotfi, R.; Tamjid, E.; Shokrgozar, M. A.; Simchi, A. Core-Sheath Gelatin Based Electrospun Nanofibers for Dual Delivery Release of Biomolecules and Therapeutics. *Mater. Sci. Eng., C* **2020**, *108*, 110432.

(8) Ibrahim, D. M.; Kakarougkas, A.; Allam, N. K. Recent Advances on Electrospun Scaffolds as Matrices for Tissue- Engineered Heart Valves. *Mater. Today Chem.* **2017**, *5*, 11−23.

(9) Zhang, S.; Guo, Y.; Dong, Y.; Wu, Y.; Cheng, L.; Wang, Y.; Xing, M.; Yuan, Q. A Novel Nanosilver/Nanosilica Hydrogel for Bone Regeneration in Infected Bone Defects. *ACS Appl. Mater. Interfaces* **2016**, *8* (21), 13242−13250.

(10) Zhang, Y.; Zhai, D.; Xu, M.; Yao, Q.; Zhu, H.; Chang, J.; Wu, C. 3D-Printed Bioceramic Scaffolds with Antibacterial and Osteogenic Activity. *Biofabrication* **2017**, *9* (2), 025037.

(11) Bhowmick, A.; Saha, A.; Pramanik, N.; Banerjee, S.; Das, M.; Kundu, P. P. Novel Magnetic Antimicrobial Nanocomposites for Bone Tissue Engineering Applications. *RSC Adv.* **2015**, *5* (32), 25437−25445.

(12) Hajipour, M. J.; Fromm, K. M.; Ashkarran, A. A.; Jimenez de Aberasturi, D. J.; Ruiz de Larramendi, I. R. d.; Rojo, T.; Serpooshan, V.; Parak, W. J.; Mahmoudi, M. Antibacterial Properties of Nanoparticles. *Trends Biotechnol.* **2013**, *31* (1), 61−62.

(13) Kapoor, G.; Saigal, S.; Elongavan, A. Action and Resistance Mechanisms of Antibiotics: A Guide for Clinicians. *J. Anaesthesiol. Clin. Pharmacol.* **2017**, *33* (3), 300.

(14) Dizaj, S. M.; Lotfipour, F.; Barzegar-Jalali, M.; Zarrintan, M. H.; Adibkia, K. Antimicrobial Activity of the Metals and Metal Oxide Nanoparticles. *Mater. Sci. Eng., C* **2014**, *44*, 278−284.

(15) Patel, A.; Gaharwar, A. K.; Iviglia, G.; Zhang, H.; Mukundan, S.; Mihaila, S. M.; Demarchi, D.; Khademhosseini, A. Highly Elastomeric Poly(Glycerol Sebacate)-Co-Poly(Ethylene Glycol) Amphiphilic Block Copolymers. *Biomaterials* **2013**, *34* (16), 3970−3983.

(16) Zaky, S. H.; Lee, K.-W.; Gao, J.; Jensen, A.; Close, J.; Wang, Y.; Almarza, A. J.; Sfeir, C. Poly(Glycerol Sebacate) Elastomer: A Novel Material for Mechanically Loaded Bone Regeneration. *Tissue Eng., Part A* **2014**, *20* (1−2), 45−53.

(17) Zaky, S. H.; Lee, K. W.; Gao, J.; Jensen, A.; Verdelis, K.; Wang, Y.; Almarza, A. J.; Sfeir, C. Poly (Glycerol Sebacate) Elastomer Supports Bone Regeneration by Its Mechanical Properties Being Closer to Osteoid Tissue Rather than to Mature Bone. *Acta Biomater.* **2017**, *54*, 95−106.

(18) Mihaila, S. M.; Gaharwar, A. K.; Reis, R. L.; Khademhosseini, A.; Marques, A. P.; Gomes, M. E. The Osteogenic Differentiation of SSEA-4 Sub-Population of Human Adipose Derived Stem Cells Using Silicate Nanoplatelets. *Biomaterials* **2014**, *35* (33), 9087−9099.

(19) Wang, Y.; Ameer, G. A.; Sheppard, B. J.; Langer, R. A Tough Biodegradable Elastomer. *Nat. Biotechnol.* **2002**, *20*, 602−606.

(20) Shirzaei Sani, E.; Portillo-Lara, R.; Spencer, A.; Yu, W.; Geilich, B. M.; Noshadi, I.; Webster, T. J.; Annabi, N. Engineering Adhesive and Antimicrobial Hyaluronic Acid/Elastin-like Polypeptide Hybrid Hydrogels for Tissue Engineering Applications. *ACS Biomater. Sci. Eng.* **2018**, *4* (7), 2528−2540.

(21) Hinderer, S.; Seifert, J.; Votteler, M.; Shen, N.; Rheinlaender, J.; Schäffer, T. E.; Schenke-Layland, K. Engineering of a Bio-Functionalized Hybrid off-the-Shelf Heart Valve. *Biomaterials* **2014**, *35* (7), 2130−2139.

(22) Fares, M. M.; Shirzaei Sani, E.; Portillo Lara, R.; Oliveira, R. B.; Khademhosseini, A.; Annabi, N. Interpenetrating Network Gelatin Methacryloyl (GelMA) and Pectin-g-PCL Hydrogels with Tunable Properties for Tissue Engineering. *Biomater. Sci.* **2018**, *6*, 2938−2950.

(23) Shirzaei Sani, E.; Kheirkhah, A.; Rana, D.; Sun, Z.; Foulsham, W.; Sheikhi, A.; Khademhosseini, A.; Dana, R.; Annabi, N. Sutureless Repair of Corneal Injuries Using Naturally Derived Bioadhesive Hydrogels. *Sci. Adv.* **2019**, *5* (3), eaav1281.

(24) Damoulis, P. D.; Drakos, D. E.; Gagari, E.; Kaplan, D. L. Osteogenic Differentiation of Human Mesenchymal Bone Marrow Cells in Silk Scaffolds Is Regulated by Nitric Oxide. *Ann. N. Y. Acad. Sci.* **2007**, *1117* (1), 367−376.

(25) Gaharwar, A. K.; Nikkhah, M.; Sant, S.; Khademhosseini, A. Anisotropic Poly (Glycerol Sebacate)-Poly (-Caprolactone) Electrospun Fibers Promote Endothelial Cell Guidance. *Biofabrication* **2015**, *7* (1), 015001.

(26) Zamani, S.; Khoee, S. Preparation of Core-Shell Chitosan/PCL-PEG Triblock Copolymer Nanoparticles with ABA and BAB Morphologies: Effect of Intraparticle Interactions on Physicochemical Properties. *Polymer* **2012**, *53* (25), 5723−5736.

(27) Masoumi, N.; Larson, B. L.; Annabi, N.; Kharaziha, M.; Zamanian, B.; Shapero, K. S.; Cubberley, A. T.; Camci-Unal, G.; Manning, K. B.; Mayer, J. E.; Khademhosseini, A. Electrospun PGS: PCL Microfibers Align Human Valvular Interstitial Cells and Provide Tunable Scaffold Anisotropy. *Adv. Healthcare Mater.* **2014**, *3* (6), 929−939.

(28) Paul, A.; Manoharan, V.; Krafft, D.; Assmann, A.; Uquillas, J. A.; Shin, S. R.; Hasan, A.; Hussain, M. A.; Memic, A.; Gaharwar, A. K.; Khademhosseini, A. Nanoengineered Biomimetic Hydrogels for Guiding Human Stem Cell Osteogenesis in Three Dimensional Microenvironments. *J. Mater. Chem. B* **2016**, *4* (20), 3544−3554.

(29) Tao, L.; Zhonglong, L.; Ming, X.; Zezheng, Y.; Zhiyuan, L.; Xiaojun, Z.; Jinwu, W. *In Vitro* and *in Vivo* Studies of a Gelatin/

Carboxymethyl Chitosan/LAPONITE® Composite Scaffold for Bone Tissue Engineering. *RSC Adv.* **2017**, *7* (85), 54100−54110.
(30) Fang, F. F.; Kim, J. H.; Choi, H. J.; Kim, C. A. Synthesis and Electrorheological Response of Nano-Sized Laponite Stabilized Poly(Methyl Methacrylate) Spheres. *Colloid Polym. Sci.* **2009**, *287* (6), 745−749.
(31) Du, J.; Zhu, J.; Wu, R.; Xu, S.; Tan, Y.; Wang, J. A Facile Approach to Prepare Strong Poly(Acrylic Acid)/LAPONITE® Ionic Nanocomposite Hydrogels at High Clay Concentrations. *RSC Adv.* **2015**, *5* (74), 60152−60160.
(32) Li, P.; Kim, N. H.; Hui, D.; Rhee, K. Y.; Lee, J. H. Improved Mechanical and Swelling Behavior of the Composite Hydrogels Prepared by Ionic Monomer and Acid-Activated Laponite. *Appl. Clay Sci.* **2009**, *46* (4), 414−417.
(33) Gaharwar, A. K.; Mukundan, S.; Karaca, E.; Dolatshahi-Pirouz, A.; Patel, A.; Rangarajan, K.; Mihaila, S. M.; Iviglia, G.; Zhang, H.; Khademhosseini, A. Nanoclay-Enriched Poly(e-Caprolactone) Electrospun Scaffolds for Osteogenic Differentiation of Human Mesenchymal Stem Cells. *Tissue Eng., Part A* **2014**, *20*, 2088−2101.
(34) Wang, S.; Zheng, F.; Huang, Y.; Fang, Y.; Shen, M.; Zhu, M.; Shi, X. Encapsulation of Amoxicillin within Laponite-Doped Poly-(Lactic- Co -Glycolic Acid) Nanofibers: Preparation, Characterization, and Antibacterial Activity. *ACS Appl. Mater. Interfaces* **2012**, *4* (11), 6393−6401.
(35) Xue, Y.; Yatsenko, T.; Patel, A.; Stolz, D. B.; Phillippi, J. A.; Sant, V.; Sant, S. PEGylated Poly(Ester Amide) Elastomer Scaffolds for Soft Tissue Engineering. *Polym. Adv. Technol.* **2017**, *28*, 1097−1106.
(36) Wang, S.; Castro, R.; An, X.; Song, C.; Luo, Y.; Shen, M.; Tomás, H.; Zhu, M.; Shi, X. Electrospun Laponite-Doped Poly-(Lactic-Co-Glycolic Acid) Nanofibers for Osteogenic Differentiation of Human Mesenchymal Stem Cells. *J. Mater. Chem.* **2012**, *22* (44), 23357.
(37) Kerativitayanan, P.; Tatullo, M.; Khariton, M.; Joshi, P.; Perniconi, B.; Gaharwar, A. K. Nanoengineered Osteoinductive and Elastomeric Scaffolds for Bone Tissue Engineering. *ACS Biomater. Sci. Eng.* **2017**, *3* (4), 590−600.
(38) Shirzaei Sani, E.; Portillo Lara, R.; Aldawood, Z.; Bassir, S. H.; Nguyen, D.; Kantarci, A.; Intini, G.; Annabi, N. An Antimicrobial Dental Light Curable Bioadhesive Hydrogel for Treatment of Peri-Implant Diseases. *Matter* **2019**, *1*, 926−944.
(39) Annabi, N.; Rana, D.; Shirzaei Sani, E.; Portillo-Lara, R.; Gifford, J. L.; Fares, M. M.; Mithieux, S. M.; Weiss, A. S. Engineering a Sprayable and Elastic Hydrogel Adhesive with Antimicrobial Properties for Wound Healing. *Biomaterials* **2017**, *139*, 229−243.
(40) Woodruff, M. A.; Hutmacher, D. W. The Return of a Forgotten Polymer—Polycaprolactone in the 21st Century. *Prog. Polym. Sci.* **2010**, *35* (10), 1217−1256.
(41) Ma, Y.; Zhang, W.; Wang, Z.; Wang, Z.; Xie, Q.; Niu, H.; Guo, H.; Yuan, Y.; Liu, C. PEGylated Poly(Glycerol Sebacate)-Modified Calcium Phosphate Scaffolds with Desirable Mechanical Behavior and Enhanced Osteogenic Capacity. *Acta Biomater.* **2016**, *44*, 110−124.
(42) Li, W.; Yu, L.; Liu, G.; Tan, J.; Liu, S.; Sun, D. Oil-in-Water Emulsions Stabilized by Laponite Particles Modified with Short-Chain Aliphatic Amines. *Colloids Surf., A* **2012**, *400*, 44−51.
(43) Bottino, M. C.; Thomas, V.; Schmidt, G.; Vohra, Y. K.; Chu, T.-M. G.; Kowolik, M. J.; Janowski, G. M. Recent Advances in the Development of GTR/GBR Membranes for Periodontal Regeneration—A Materials Perspective. *Dent. Mater.* **2012**, *28* (7), 703−721.
(44) Thomas, M. V.; Puleo, D. A. Infection, Inflammation, and Bone Regeneration: A Paradoxical Relationship. *J. Dent. Res.* **2011**, *90* (9), 1052−1061.
(45) Giuliani, A.; Pirri, G.; Nicoletto, S. Antimicrobial Peptides: An Overview of a Promising Class of Therapeutics. *Open Life Sci.* **2007**, *2* (1), 1−33.
(46) Batoni, G.; Maisetta, G.; Esin, S. Antimicrobial Peptides and Their Interaction with Biofilms of Medically Relevant Bacteria. *Biochim. Biophys. Acta, Biomembr.* **2016**, *1858* (5), 1044−1060.
(47) Eriksen, T. H. B.; Skovsen, E.; Fojan, P. Release of Antimicrobial Peptides from Electrospun Nanofibres as a Drug Delivery System. *J. Biomed. Nanotechnol.* **2013**, *9* (3), 492−498.
(48) Stallmann, H. P.; Roo, R. de; Faber, C.; Amerongen, A. V. N.; Wuisman, P. I. J. M. In Vivo Release of the Antimicrobial Peptide HLF1−11 from Calcium Phosphate Cement. *J. Orthop. Res.* **2008**, *26* (4), 531−538.
(49) Cheng, H.; Yue, K.; Kazemzadeh-Narbat, M.; Liu, Y.; Khalilpour, A.; Li, B.; Zhang, Y. S.; Annabi, N.; Khademhosseini, A. Mussel-Inspired Multifunctional Hydrogel Coating for Prevention of Infections and Enhanced Osteogenesis. *ACS Appl. Mater. Interfaces* **2017**, *9* (13), 11428−11439.
(50) Wang, S.; Wu, Y.; Guo, R.; Huang, Y.; Wen, S.; Shen, M.; Wang, J.; Shi, X. Laponite Nanodisks as an Efficient Platform for Doxorubicin Delivery to Cancer Cells. *Langmuir* **2013**, *29* (16), 5030−5036.
(51) Geurts, J.; Chris Arts, J. J.; Walenkamp, G. H. I. M. Bone Graft Substitutes in Active or Suspected Infection. Contra-Indicated or Not? *Injury* **2011**, *42*, S82−S86.
(52) Fernandes, A.; Dias, M. The Microbiological Profiles of Infected Prosthetic Implants with an Emphasis on the Organisms Which Form Biofilms. *J. Clin. DIAGNOSTIC Res.* **2013**, *7* (3), 219−223.
(53) Shi, J.; Liu, Y.; Wang, Y.; Zhang, J.; Zhao, S.; Yang, G. Biological and Immunotoxicity Evaluation of Antimicrobial Peptide-Loaded Coatings Using a Layer-by-Layer Process on Titanium. *Sci. Rep.* **2015**, *5* (1), 16336.
(54) Sonohara, R.; Muramatsu, N.; Ohshima, H.; Kondo, T. Difference in Surface Properties between Escherichia CoZi and Staphylococcus Aureus as Revealed by Electrophoretic Mobility Measurements. *Biophys. Chem.* **1995**, *55*, 273−277.
(55) *Bacillus Subtilis and Its Closest Relatives*; Sonenshein, A. L., Hoch, J. A., Losick, R., Eds.; American Society of Microbiology, 2002. DOI: 10.1128/9781555817992.
(56) Zhao, L.; Wang, H.; Huo, K.; Cui, L.; Zhang, W.; Ni, H.; Zhang, Y.; Wu, Z.; Chu, P. K. Antibacterial Nano-Structured Titania Coating Incorporated with Silver Nanoparticles. *Biomaterials* **2011**, *32* (24), 5706−5716.
(57) Schexnailder, P. J.; Gaharwar, A. K.; Bartlett, R. L., II; Seal, B. L.; Schmidt, G. Tuning Cell Adhesion by Incorporation of Charged Silicate Nanoparticles as Cross-Linkers to Polyethylene Oxide. *Macromol. Biosci.* **2010**, *10* (12), 1416−1423.
(58) Thies, R. S.; Bauduy, M.; Ashton, B. A.; Kurtzberg, L.; Wozney, J. M.; Rosen, V. Recombinant Human Bone Morphogenetic Protein-2 Induces Osteoblastic Differentiation in W-20−17 Stromal Cells. *Endocrinology* **1992**, *130* (3), 1318−1324.
(59) Pujari-Palmer, S.; Lind, T.; Xia, W.; Tang, L.; Karlsson Ott, M. Controlling Osteogenic Differentiation through Nanoporous Alumina. *J. Biomater. Nanobiotechnol.* **2014**, *05* (02), 98−104.
(60) Seibel, M. J. Biochemical Markers of Bone Turnover: Part I: Biochemistry and Variability. *Clin. Biochem. Rev.* **2005**, *26* (4), 97−122.
(61) Kim, S.; Tsao, H.; Kang, Y.; Young, D. A.; Sen, M.; Wenke, J. C.; Yang, Y. In Vitro Evaluation of an Injectable Chitosan Gel for Sustained Local Delivery of BMP-2 for Osteoblastic Differentiation. *J. Biomed. Mater. Res., Part B* **2011**, *99B* (2), 380−390.
(62) Wei, S.; Gao, X.; Zhang, X.; Song, J.; Xu, X.; Xu, A.; Wang, M.; Xie, B.; Huang, E.; Deng, F. Osteoinductive Peptide-Functionalized Nanofibers with Highly Ordered Structure as Biomimetic Scaffolds for Bone Tissue Engineering. *Int. J. Nanomed.* **2015**, 7109.
(63) Kim, J. H.; Liu, X.; Wang, J.; Chen, X.; Zhang, H.; Kim, S. H.; Cui, J.; Li, R.; Zhang, W.; Kong, Y.; Zhang, J.; Shui, W.; Lamplot, J.; Rogers, M. R.; Zhao, C.; Wang, N.; Rajan, P.; Tomal, J.; Statz, J.; Wu, N.; Luu, H. H.; Haydon, R. C.; He, H. C. Wnt Signaling in Bone Formation and Its Therapeutic Potential for Bone Diseases. *Ther. Adv. Musculoskeletal Dis.* **2013**, *5* (1), 13−31.
(64) Gaharwar, A. K.; Schexnailder, P. J.; Kline, B. P.; Schmidt, G. Assessment of Using Laponite Cross-Linked Poly(Ethylene Oxide)

for Controlled Cell Adhesion and Mineralization. *Acta Biomater.* **2011**, *7* (2), 568−577.

https://dx.doi.org/10.1021/acsabm.0c00250
ACS Appl. Bio Mater. 2020, 3, 3313−3325